iScience

CellPress
OPEN ACCESS

Article

Human fetal membrane-mesenchymal stromal cells generate functional spinal motor neurons *in vitro*

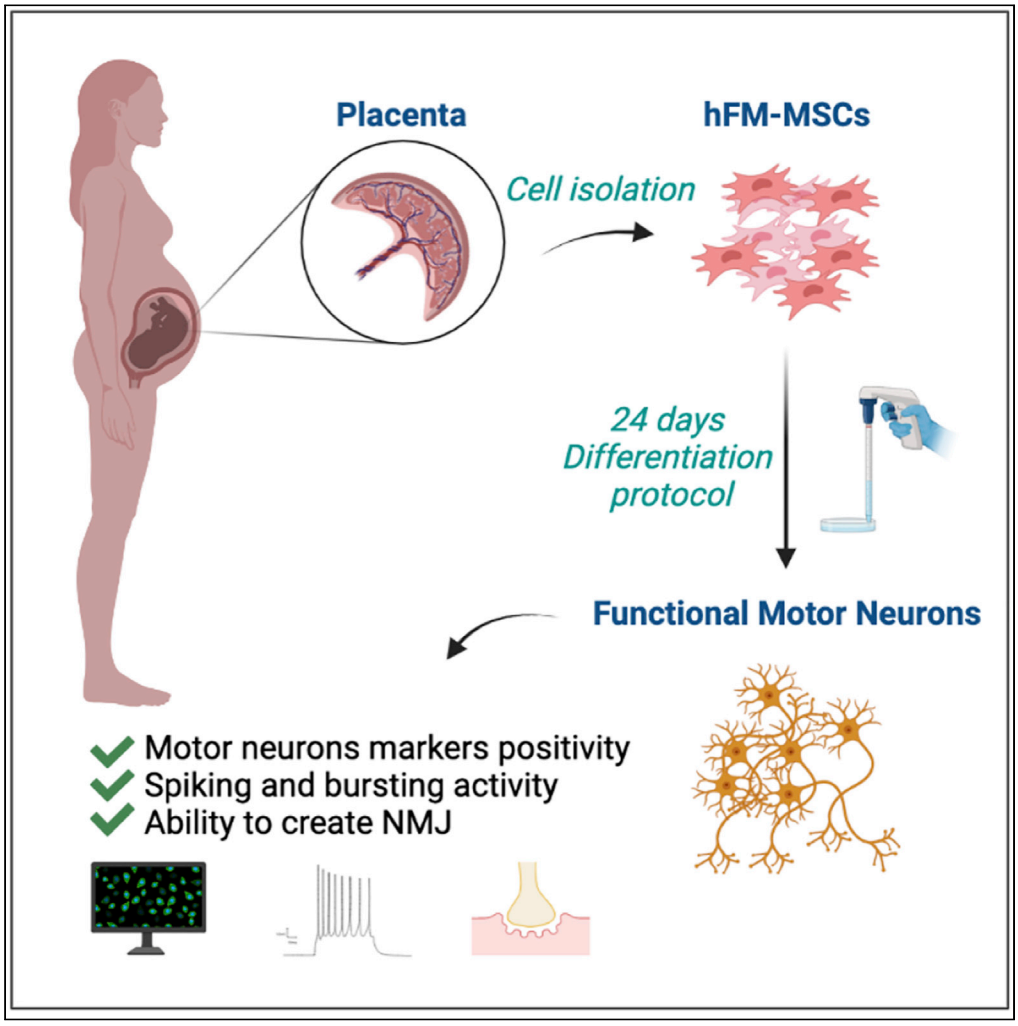

Giulia Gaggi, Andrea Di Credico, Simone Guarnieri, Maria Addolorata Mariggiò, Patrizia Ballerini, Angela Di Baldassarre, Barbara Ghinassi

a.dibaldassarre@unich.it

Highlights

hFM-MSCs overcome their mesodermal restriction generating ectodermal-derived cells

hFM-MSCs can differentiate into functional spinal MNs

hFM-MSC derived spinal MNs create a functional NMJ with myotubes

A spontaneous electrical activity is registered during the maturation phase

Gaggi et al., iScience *25*, 105197
October 21, 2022
https://doi.org/10.1016/j.isci.2022.105197

iScience

CellPress
OPEN ACCESS

Article

Human fetal membrane-mesenchymal stromal cells generate functional spinal motor neurons *in vitro*

Giulia Gaggi,[1,2,5] Andrea Di Credico,[1,2,5] Simone Guarnieri,[2,3] Maria Addolorata Mariggiò,[2,3] Patrizia Ballerini,[4] Angela Di Baldassarre,[1,2,6,*] and Barbara Ghinassi[1,2]

SUMMARY

Human fetal membrane mesenchymal stromal cells (hFM-MSCs) are a cell population easily isolable from the amniochorionic membrane of term placentas, without ethical issues or safety limitations. We previously reported that hFM-MSCs share some epigenetic characteristics with pluripotent stem cells and can overcome the mesenchymal commitment. Here, we demonstrated that hFM-MSCs can give rise to spinal motor neurons by the sequential exposure to specific factors that induced a neuralization, caudalization and ventralization of undifferentiated cells, leading to a gradual gene and protein upregulation of early and late MN markers. Also, spontaneous electrical activity (spikes and bursts) was recorded. Finally, when co-cultured with myotubes, differentiated MNs were able to create functional neuromuscular junctions that induced robust skeletal muscle cell contractions. These data demonstrated the hFM-MSCs can generate a mature and functional MN population that may represent an alternative source for regenerative medicine, disease modeling or drug screening.

INTRODUCTION

Spinal motor neurons (MNs) are a highly specialized type of cells that reside in the ventral horns of the spinal cord and project axons to muscles to generate contractile activity. The embryonic development of MNs is a complex process involving many steps (Price and Briscoe, 2004; Cave and Sockanathan, 2018). During the initial phase, when the neural tube is specified into forebrain, midbrain, hindbrain and spinal cord, a gradient of retinoic acid (RA), WNTs and fibroblast growth factors (FGFs) allows the delineation of the boundary between the spinal cord-hindbrain and midbrain along the anteroposterior axis (Price and Briscoe, 2004; Davis-Dusenbery et al., 2014), whereas the Fibroblast growth factor 2 (Fgf2) and Growth differentiation factor 11 (Gdf11) within the dorsoventral axis allow the specification of MN progenitor cells. Then, Sonic hedgehog (Shh) and the BMP/TGF-β derived from the roof plate allow the consolidation of MN progenitors identity activating downstream transcription factors, such as Paired Box 6 (Pax6) (Akazawa, 2004; Davis-Dusenbery et al., 2014). Finally, Olig2 induces the expression of Neurogenin 2, which promotes the MNs maturation, characterized by the exit from cell cycle and the expression of late markers such as Insulin gene enhancer protein 1/2 (Isl1/2) and Homeobox HB9 (Hb9) (Price and Briscoe, 2004; Davis-Dusenbery et al., 2014).

Degeneration of MNs is implicated in a great number of devastating diseases, including spinal muscular atrophy, amyotrophic lateral sclerosis, and Charcot-Marie-Tooth (Stifani, 2014; Du et al., 2015), all characterized by the progressive loss of function of neurons and their death. The contribution of the stem cells to field of the neurodegenerative diseases has been explored extensively over the past few years, and the possibility to use stem cells for replacing lost spinal MNs or for the development of *in vitro* disease models for pathogenesis studies and drug screening remains appealing. To date, functionally mature human (h) MNs have been obtained only from embryonic (hESCs) and induced pluripotent stem cells (hiPSCs), but unfortunately, the use of these cellular models raises ethical and/or safety limitations (Di Baldassarre et al., 2018; Moradi et al., 2019). For this reason, the identification of an alternative source of stem cells that can efficiently differentiate into MNs is crucial.

Fetal membrane derived-mesenchymal stem cells (FM-MSCs) represent a cell population that can be easily isolated from the amniochorionic membrane of the placenta after birth (Díaz-Prado et al., 2011; Chatgilialoglu et al., 2017; Gaggi et al., 2019). hFM-MSCs originate from the epiblast-derived extraembryonic

[1]Department of Medicine and Sciences of Aging, "G. d'Annunzio" University of Chieti-Pescara, Via dei Vestini, 31, 66100 Chieti, Italy

[2]Reprogramming and Cell Differentiation Lab, Center for Advanced Studies and Technology (CAST), "G. d'Annunzio" University of Chieti-Pescara, Via dei Vestini, 31, 66100 Chieti, Italy

[3]Department of Neuroscience, Imaging and Clinical Sciences, "G. d'Annunzio" University of Chieti-Pescara, Via dei Vestini, 31, 66100 Chieti, Italy

[4]Department of Innovative Technologies in Medicine and Dentistry, "G. d'Annunzio" University of Chieti-Pescara, Via dei Vestini, 31, 66100 Chieti, Italy

[5]These authors contributed equally

[6]Lead contact

*Correspondence: a.dibaldassarre@unich.it

https://doi.org/10.1016/j.isci.2022.105197

Table 1. hFM-MSC phenotypic characterization

Marker	Positive cells (%)
Pluripotent stem cell markers	
OCT4	25.2 ± 8.3
SSEA4	18.3 ± 4.1
SOX2	28.9 ± 4.6
NANOG	88.1 ± 5.7
TRA1-60	4.1 ± 1.6
C-KIT	1.9 ± 1.2
Mesenchymal stem cell markers	
CD90	88.7 ± 6.4
CD73	92.1 ± 4.5
CD105	84.2 ± 8.5
CD44	94.4 ± 2.3
Hematopoietic cell markers	
CD45	negative
CD14	negative

mesoderm (Saykali et al., 2019) and, together with the amniotic epithelium, form the fetal membrane that surrounds the fetus providing endocrine, antimicrobial and transportation functions. In particular, the FM-MSCs populations seem to deeply contribute to the development of fetal-maternal tolerance, as when cultured *in vitro* they suppress the cytotoxic activity of T and Natural Killer cells (Magatti et al., 2019). These placental derived stem cells represent a population very appealing for clinical and research purposes, as their use raises neither ethical concerns, deriving from discarded material, nor safety issues, being not tumorigenic and low immunogenic (Consentius et al., 2015; Papait et al., 2020). Generally considered multipotent and committed to the mesodermal lineage (Sancricca, 2010; Chatgilialoglu et al., 2017), hFM-MSCs also express the pluripotent master genes *OCT4*, *NANOG*, and *SOX2*, and share some epigenetic traits with hiPSCs. (Gaggi et al., 2020a,2020b). Basing on these biological characteristics that put the hFM-MSCs at the intersection between embryonic and adult stem cells, we checked whether hFM-MSCs can overcome their mesenchymal destiny and differentiate into an ectodermal progeny: in particular, we evaluated their ability to generate functional MNs, to contribute to paving the way to treatment of the MN degenerative diseases.

RESULTS

hFM-MSCs were characterized by flow cytometry between passages 2 and 4. As in previous studies (Gaggi et al., 2020a), we demonstrated that they were negative for the hematopoietic markers CD45 and CD14, whereas they expressed the pluripotent stem cell markers SSEA4, OCT4, SOX2, NANOG, c-KIT and Tra-1–60 and the mesenchymal stem cell markers CD90 and CD73 (Table 1).

hFM-MSCs can generate phenotypically characterized MNs

To elucidate whether hFM-MSCs can be driven toward the MN fate, cells were grown as embryoid bodies (EBs) and exposed to small molecules known to induce both hiPSCs and hESCs differentiating into MNs (Maury et al., 2015): first cells underwent the classical dual SMAD inhibition protocol to induce the neural commitment (Chambers et al., 2009), then the MN induction was obtained exposing the cells to RA and Smoothened receptor agonists (SAG), that activate the SHH signaling and induce the acquisition of MN identity (Stifani, 2014); finally, maturation of differentiated MNs was induced by neurotrophic factors (Figure 1A). As morphology is an important indicator of cell function and differentiation (Harkness et al., 2019), changes in the cellular shape during the different phases of the cell culture were monitored (Figures 1B and 1C): hFM-MSCs, which have a fibroblastic shape, were able to form small (about 100 μm) EBs, that were cultured up to 16 days to induce the MN commitment; once dissociated, EBs derived cells evidenced the typical neuronal morphology; finally, the maturation phase was characterized by an increasing number, size and complexity of neurites and cell-cell connections (day 24), whereas after 40 days of culture, cells

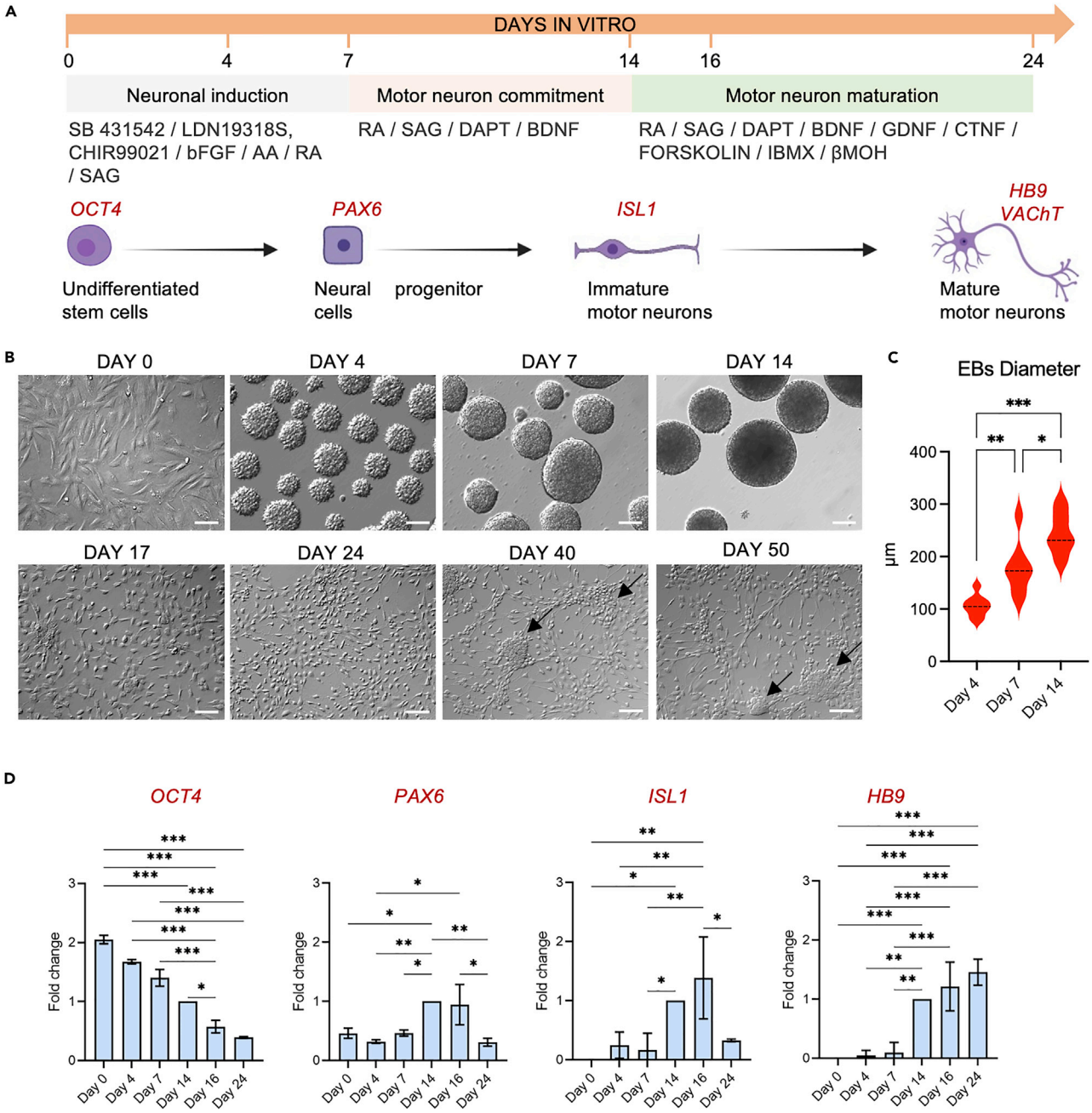

Figure 1. Phenotypic analysis of hFM-MSCs during the differentiation into MNs

(A) Schematic representation of the key points of the motor neuron differentiation. The different phases of the differentiation steps and the small molecules used are reported in the timeline, whereas the specific MNs genes are indicated in red.

(B) Morphological analysis of different differentiation steps. Black arrows indicate the clusterization of hFM-MSC-derived MNs. Magnification 10x, scale bar 100 μm. Pictures are representative of 5 independent experiments from 5 different biological samples.

(C) EBs diameter. The graphs show the Mean ± SD (n = 3 *p <0.05, **p =0.001, ***p<0.001).

(D) Gene expression of *OCT4, PAX6, ISL1* and *HB9* at different time points of the differentiation process, as indicated. Data are expressed as fold changes (Mean ± SD) respect to day 14. *18S* was used as reference gene (n = 3, *p <0.05, **p =0.001, ***p<0.001). AA, Ascorbic acid. RA, retinoid acid. SAG, Smoothened receptor agonists. bFGF, basic Fibroblast growth factor . BDNF, Brain-derived neurotrophic factor. GDNF, Glial cell line-derived neurotrophic factor. CTNF, Ciliary neurotrophic factor. βOH, β-mercaptoethanol.

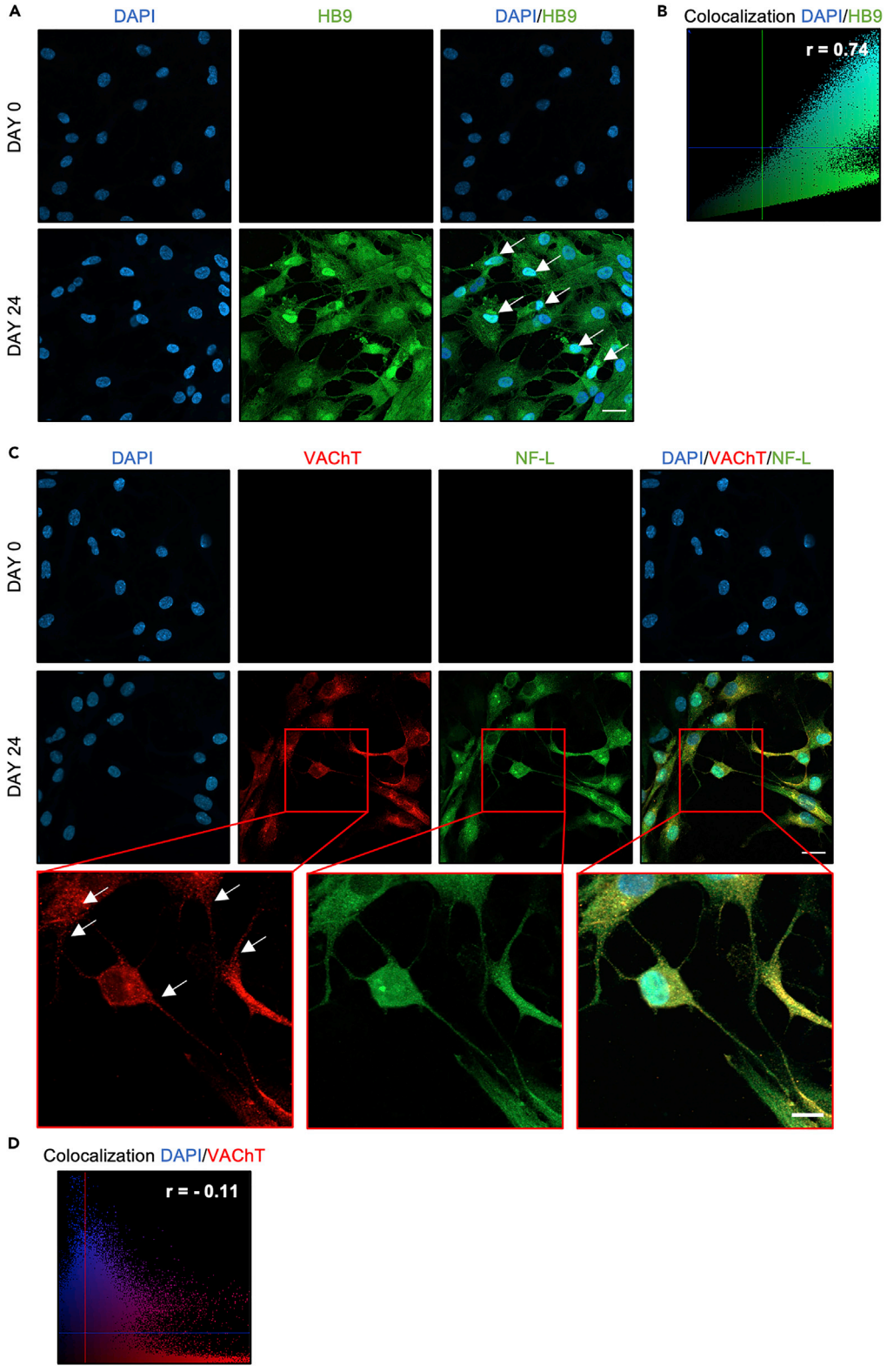
A
DAPI
HB9
DAPI/HB9
DAY 0
DAY 24
B
Colocalization DAPI/HB9
r = 0.74
C
DAPI
VAChT
NF-L
DAPI/VAChT/NF-L
DAY 0
DAY 24
D
Colocalization DAPI/VAChT
r = - 0.11

Figure 2. Immunofluorescence analysis of MN-specific markers

(A) HB9 (green fluorescence) in undifferentiated cells (day 0) and after 24 days of culture. The nuclei were counterstained with DAPI (blue). White arrows indicate the nuclear localization of HB9 in the differentiated cells. Original magnification: 40x, scale bar 20 μm. Images are representative of 3 independent experiments.

(B) HB9 fluorescence intensity graph; data are expressed as Mean ± SD (n = 3, ***p<0.001).

(C) ScatterPlot of the colocalization between blue (nuclei) and green (HB9) signal calculated using the Pearson's coefficient (r= 0.74).

(D) immunofluorescence for vAChT (red) and NF-L (green) in undifferentiated cells (day 0) and after 24 days of culture. The nuclei were counterstained with DAPI (blue). Original magnification: 40x, scale bar 20 μm. Red rectangle represents an enlarged area: magnification 60x, scale bar 10 μm. Images are representative of 3 independent experiments.

The graphs show the Mean ± SD of 3 diverse, randomly selected fields of 3 independent experiments. ***p<0.001.

Scatterplot of the colocalization between blue (nuclei) and red (vAChT) signal calculated by Pearson's coefficient (r= −0.11).

started changing their spatial organization by clustering in islets of neurons, similar to that formed by hiPSCs-derived MNs. During the differentiation steps, we examined various genes, whose expression is known to be pivotal in the acquisition of MN phenotype. The qPCR (primer sequences reported in Table 3) data evidenced that the stemness marker *OCT4* gradually decreased, as expected, whereas the MN-specific markers *PAX6, ISL1* and *HB9* increased. More specifically, *PAX6*, one of the earliest markers in MN differentiation, detectable at low levels in undifferentiated hFM-MSCs, reached its highest expression during the second week of differentiation and decreased thereafter; *ISL1* showed a similar trend, whereas *HB9*, a late MN marker, unexpressed in undifferentiated cells, showed its peak in the last phases of the differentiation (Figure 1D).

To confirm the acquisition of the MN phenotype, after 24 days of differentiation we analyzed the expression and the localization of proteins involved in the consolidation of MN identity, such as the nuclear factor HB9, the vesicular acetylcholine transporter (vAChT) and the Neurofilament light chain (NF-L). Immunofluorescence analyses revealed that all these markers, undetectable in undifferentiated hFM-MSCs, were expressed during the maturing phase by the majority of the cells (Figure 2): HB9, the transcription factor considered the gold standard for the identification of mature MNs (Alves et al., 2015), was diffusely present and localized mainly in the cell nuclei; the cytoskeletal structural protein NF-L strongly marked the cytoplasm of most of the differentiated cells, whereas vAChT depicted its typical vesicular-staining pattern inside the soma and neurites of the MNs, leaving unmarked the nuclei. Percentages of cell positivity and fluorescence intensity are reported in Table 2.

These data demonstrated that hFM-MSCs were able to differentiate with high efficiency into cells characterized by the morphological and phenotypical features of MNs.

hFM-MSC-derived MNs show spontaneous electrical activity and establish functional neuromuscular junctions

We then checked whether the morphological and phenotypical changes were accompanied by the acquisition of specific electrical properties. For this purpose, after the dissociation (Day 16), cells were seeded on multi-electrode array (MEA) plates, a non-invasive technology using biosensors that detects the electrophysiological activity of neurons in real-time through electrodes implanted in the tissue culture wells (Figure 3A). During the cell culture, only sporadic action potentials were recorded for up to 7 weeks; then, a robust increment of the electrical activity was observed, with a significant increase in the mean firing rate (Figure 3B), indicating a functional maturation of the neurons. Accordingly, a substantial burst increase (clusters of spikes) was also detected, as highlighted by the augmented bursting frequency and duration (Figures 3B and3C).

As the functional output of MNs is the contraction of skeletal muscle cells, we then evaluated whether hFM-MSC-derived MNs were able to form physiologically relevant connections with myotubes. After the dissociation, cells were pre-loaded with a long-lasting blue vital staining and seeded on the top of differentiated C2C12 myotubes to evaluate the possible formation of neuromuscular junctions (NMJ). After one week of co-culture, the presence of potential NMJs was investigated immunocytochemically by analyzing whether the motor neuron axonal processes (labeled with vital blue staining) contacted the muscular post-synaptic nicotine acetylcholine receptors (AChRs) marked with a fluorescent α-bungarotoxin (BTX), a polypeptide which binds specifically to muscle AChRs. Immunofluorescence analyses demonstrated that the neuronal

Table 2. hFM-MSC-derived MN phenotypic characterization

	Positive cells (% of the total)		Fluorescence intensity (MFI)	
Marker	Day 24	Day 50	Day 24	Day 50
Tubulin βIII	77.3 ± 3.2	73.0 ± 2.2	1016.7 ± 70.1	1002.4 ± 66.4
ISL1	81.3 ± 5.4	80.1 ± 4.1	1116.5 ± 83.2	1222.8 ± 74.3
NF-L	87.6 ± 2.8	89.5 ± 5.1	14387 ± 87.1	14464.8 ± 79.9
HB9	70.8 ± 5.7	73.3 ± 4.5	11393.7 ± 74.2	9775.8 ± 91.0
ChAT	78.5 ± 6.2	80.1 ± 5.8	881.74 ± 69.2	1212.1 ± 70.0[a]
vAChT	80.2 ± 3.3	84.4 ± 4.6	851.5 ± 75.5	1247.0 ± 68.4[a]
SV2	81.4 ± 4.2	83.4 ± 3.3	854.6 ± 73.3	1110.4 ± 70.3[a]

[a]$p<0.05$ vs day 24.

terminal arbors ended on the AChRs present on the myotubes. In addition, for a better characterization of the NMJ, we stained the hFM-MSC-derived MNs also with an antibody against SV2, a pre-synaptic protein found on secretory vesicles that localizes both in the cell soma and along the axons (Nowack et al., 2010). Data obtained showed an attempt of AChR clusterization and an alignment of SV2 and α-BTX, suggesting that hFM-MSC-derived MNs are competent to form NMJ (Figure 3D).

The functionality of these NMJ was then suggested by the evidence that although only sporadic and weak contractions were observed in C2C12 myotubes maintained in single cultures (Video S1), a robust contractile activity was recorded after a week of co-culture with hFM-MSC-derived MNs (Video S2). The degree of the C2C12 myotube contractions was evaluated by tracking the cells on the recorded videos and measuring the covered distance: in absence of hFM-MSC-derived MNs, the myotubes carried out only small movements, whereas when in co-culture the cell track evidenced significant shifts at high frequency (Figure 3E).

To confirm that the contractile activity observed was effectively because of the presence of a functional NMJ, we treated the co-culture with the α-BTX, which binds AChR with high affinity blocking their post-synaptic activity causing muscle paralysis (Bauer et al., 2022). Data showed that the contractions of myotubes co-cultured with hFM-MSC-derived MNs were completely abolished after the incubation with α-BTX (Video S3). We also checked whether the contractile activity observed in the co-culture was evoked by NMJ activation and not by crosstalk orchestrated via the secretion of trophic factors released in the microenvironment: for this purpose, we set up a non-contacting co-culture in which hFM-MSC-derived MNs and C2C12 myotubes were cultured together in chambered wells that allow the cells to grow separately sharing the medium and the secreted factors. After a week, the intracellular Ca^{2+} transients were measured in the myotubes cultured alone, in the non-contacting co-culture, and in the classical co-culture (Figure 3F): we registered only irregular and slow intracellular Ca^{2+} oscillations in myotubes cultured alone, as expected. A similar slow kinetics in intracellular calcium oscillation were recorded in the non-contacting system, whereas regular and high frequency Ca^{2+} waves were detected in myotubes cultured in contact with hFM-MSC-derived MNs. In accordance with the Ca^{2+} transients analysis, no contractile activity was microscopically evident in non-contacting co-culture (data not shown). These data prove that hFM-MSC-derived MNs are able to establish functional NMJ with myotubes.

Maturation of hFM-MSC-derived MNs is accompanied by changes in the expression levels of the neurotransmission components

Because the functional maturation of the hFM-MSC-derived MNs was observed not before 7 weeks, we monitored the expression of the markers commonly used for assessing neuronal maturity until day 50 of culture. The immunofluorescence data showed that after 24 days of differentiation most of the cells (about 80%) were positive for all the MN markers analyzed and that the percentage of the positive cells remained constant until day 50 (Table 2). However, although Tubulin βIII, ISL1 and HB9 maintained also comparable expression levels, the later stage markers ChAT, vAChT and SV2 showed a statistically significant increase of their fluorescence intensity from day 24 to day 50 (Figure 4 and Table 2). These data evidenced that hFM-MSC MN maturation phase is characterized by an upregulation of the molecular machinery required for ACh synthesis and release.

Table 3. qPCR primer sequences

Gene	Sequence (5′ - 3′)	Reference
Endo-*OCT4*-FW	GGGTTTTTGGGATTAAGTTCTTCA	(Aasen et al., 2008)
Endo-*OCT4*-RV	GCCCCCACCCTTTGTGTT	
PAX6-FW	CCAACTCCATCAGTTCCAACG	(Gaggi et al., 2022)
PAX6-RV	GGCTGCTAGTCTTTCTCGGG	
HB9-FW	GCACCAGTTCAAGCTCAAC	(Yu et al., 2020)
HB9-RV	GCTGCGTTTCCATTTCATCC	
ISL1-FW	GCCTGCTTTTCAGCAACTGG	Primer Blast
ISL1-RV	GCCTCAATAGGACTGGCTACC	
18S-FW	CATGGCCGTTCTTAGTTGGT	(Rubino et al., 2021)
18S-RV	CGCTGAGCCAGTCAGTGTAG	

DISCUSSION

Because of severe disability and the high fatality rate of the MNs degenerative diseases, it is of great importance to develop cellular models that allow drug screening assays and lay the foundation for their possible use in regenerative medicine. hESCs or hiPSCs can generate MNs with very high efficiency but their use in biomedical research and regenerative medicine raises ethical and safety issues (Ghule et al., 2011; Di Baldassarre et al., 2018). The four transcription factors (OCT4, SOX2, c-MYC, and KLF4), critical for the reprogramming to obtain iPSCs, are frequently overexpressed in tumors, and mice transplanted with iPSCs are prone to develop cancers, including teratoma. Therefore, the genomic instability of iPSCs is a major concern that could produce huge impact on their eventual clinical use (Zhang et al., 2018). *In vitro* cultured hFM-MSCs may represent an appealing alternative to hESCs or hiPSCs because they display negligible immunogenicity, demonstrate no evidence for genetic instability, while presenting no ethical concerns: In particular, they are low immunogenic as express low levels of MHC class I, are negative for MHC class II antigens and exert immunomodulatory activities by reducing the expression of inflammatory cytokines, and reducing the T cytotoxicity (Yang et al., 2019); moreover, they have great expansion capacity (considerably faster doubling time than adult MSCs), do not present genomic instability and, unlike ESC or iPCSs, do not form teratomas when transplanted in immunocompromised animal models (Rennie et al., 2012; Pipino et al., 2013). Recently, hMSCs were also isolated from the human embryonic H9 cell line and it has been observed that, unlike their parental cell line, they do not have the capacity to form teratomas (Rojas et al., 2020). We already reported that hFM-MSCs transcriptional profile includes some embryonic markers, such as *KLF4*, *OVOL1*, and *ESG1*, genes known to be abundantly and uniquely expressed in hESC and hiPSCs (Gaggi et al., 2020b). It is then probable that hFM-MSCs represent the intersection between the embryonic and the adult stem cells, being plastic as the pluripotent and safe as the multipotent stem cells.

Although there is evidence that hFM-MSCs express some neuronal markers (Maraldi et al., 2014; Mitchell et al., 2003; Weiss et al., 2006; Witkowska-Zimny and Wrobel, 2011), a fully differentiated MN progeny from placental cells has never been obtained. Here, we reported for the first time that hFM-MSCs can give rise efficiently to a population of functional MNs. The finding that hFM-MSCs were able to overcome their mesodermic restriction to generate MNs, which are an ectoderm derivate, using a protocol developed for pluripotent cells, is very intriguing. One possible explanation for this observation is that hFM-MSCs are cells with an intermediate phenotype straddling the pluripotency and the multipotency status which make them responsive to the small molecule protocol. This hypothesis is supported by the fact that they express concomitantly both pluripotency and mesenchymal markers. However, the possibility that cultured hFM-MSCs still maintain enough plasticity to be "reprogrammed" to a pluripotent-like state via the EBs formation and/or by specific culture conditions cannot be ruled out. Indeed, as with all MSCs derived from other tissues, the innate identity of hFM-MSCs remain to be elucidated: it has been suggested a possible vasal origin of the MSCs, as both pericytes and perivascular (adventitial) cells, when cultured *in vitro*, establish an MSC population that is undistinguishable from the conventional bone marrow derived MSCs. The association with the vasculature would allow the MSCs to respond quickly to injuries and would explain the wide distribution of these cells (Pittenger et al., 2019) and the references herein); therefore, in this scenario, the hFM-MSCs might be derived from the vasculature of the amniochorionic membrane. If their origins are still unclear, also the "*in vivo*" potential of hFM-MSCs remain obscure: in particular,

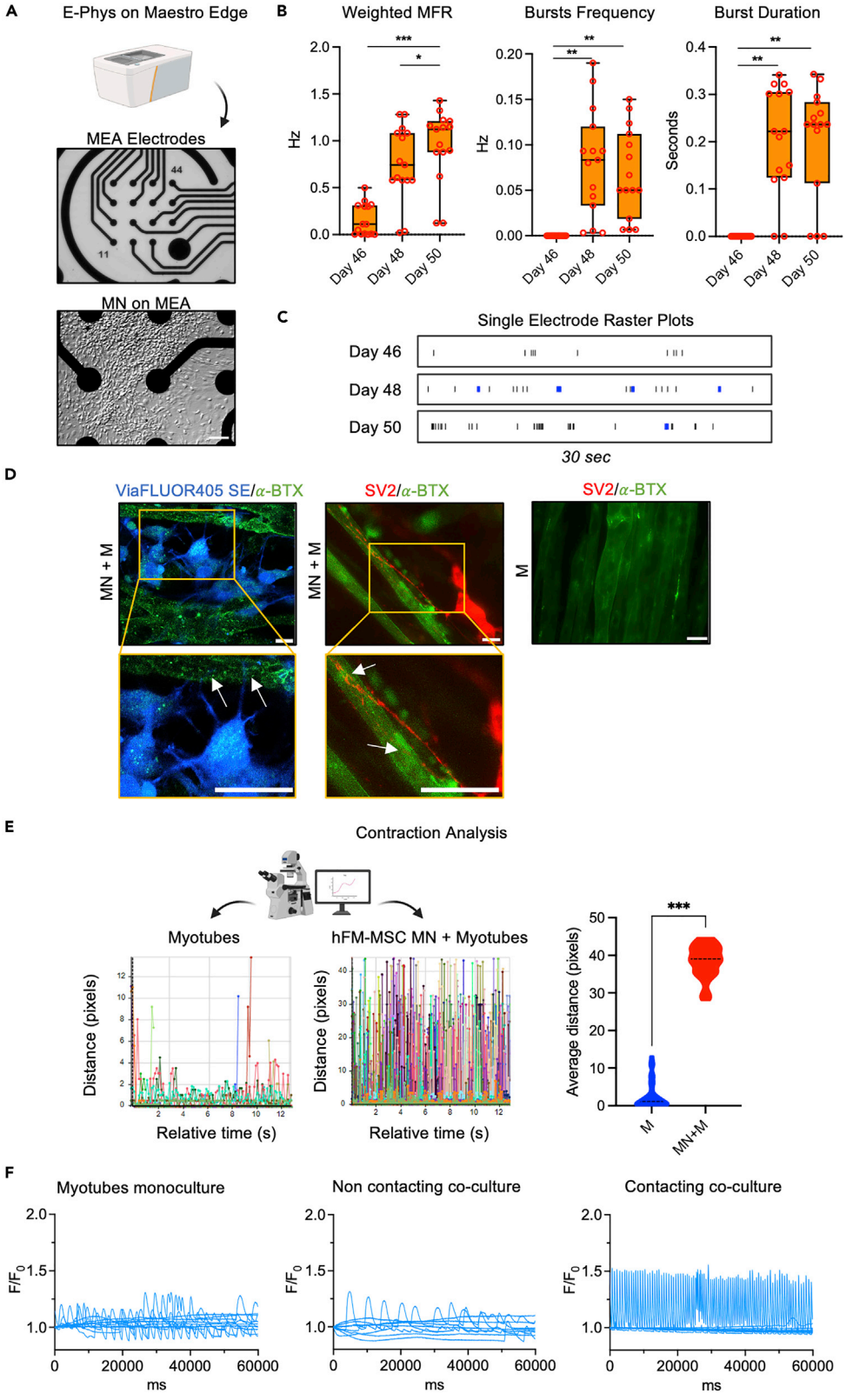
A
E-Phys on Maestro Edge
MEA Electrodes
MN on MEA
B
Weighted MFR
Bursts Frequency
Burst Duration
Hz
Seconds
Day 46
Day 48
Day 50
C
Single Electrode Raster Plots
30 sec
D
ViaFLUOR405 SE/α-BTX
SV2/α-BTX
MN + M
M
E
Contraction Analysis
Myotubes
hFM-MSC MN + Myotubes
Distance (pixels)
Relative time (s)
Average distance (pixels)
F
Myotubes monoculture
Non contacting co-culture
Contacting co-culture
F/F0
ms

Figure 3. Functional characterization of hFM-MSC-derived MNs

(A) The MEA well with and without differentiating cells. Magnification: 4x (upper image) and 10x (lower image), scale bar 100 μm.

(B) Spontaneous electrophysiological activity (weighted mean firing rate, burst frequency and burst duration) measured by MEA. Data are expressed as mean ± SEM (n = 5, *p<0.05; ** <0.01; *** <0.001).

(C) Single electrode raster plots representative of the electrical activity pattern recorded at day 46, 48, 50.

(D) NMJ detection in the co-culture of differentiating hFM-MSC, pre-loaded with a long-lasting vital dye (ViaFluor SE 405, blue fluorescence, left panels) or stained with SV2 (red fluorescence, middle panels, and C2C12 myotubes on which AChRs are marked by α-BTX (green fluorescence). The right panel shows C2C12 myotubes cultured without differentiating hFM-MSCs, stained with α-BTX (green fluorescence) and SV2 (red fluorescence). White arrows indicate neuronal terminals ending on the α-BTX (AChRs), where the attempt of AChR clusterization is shown by the increased fluorescence in the point of contact. Original magnification: 40x, scale bar 20μm; enlarged area in red rectangle: 60x.

(E) Video analysis of the muscle cell contractions in single culture of myotubes or in hFM-MSC-derived MNs plus myotubes co-culture. The movements of different points were tracked and quantified by Celleste Image Analysis Software. Graphs are representative of the distance covered by moving points inside five differently ROI. The violin plot shows the quantification of the myotube contraction ***p < 0.01.

(F) Quantitative analysis of spontaneous intracellular Ca^{2+} activities in FLUO-4 loaded myotubes cultured alone (M, myotubes monoculture), and in Transwell cell cultured condition (noncontacting co-culture) and directly contacting co-culture between hFM-MSC MN and C2C12 myotubes (MN + M), as indicated.

whether this ability to generate MNs represents one "innate" characteristic or rather the acquisition of an "*in vitro*" phenotype because of the multi-passages in defined culture condition remain to be elucidated. However, although much remains to be gained in terms of scientific knowledge about the identity and the complex biology of hFM-MSCs, their commitment toward the spinal MNs lineage represents an important foundation for future studies and clinical application.

The ability to generate EBs is commonly considered a feature of pluripotency signature of ESC and iPSCs (Antonucci et al., 2014). EBs are three-dimensional (3D) aggregates of pluripotent stem cells that comprise the three embryonic germ layers (Itskovitz-Eldor et al., 2000); providing a suitable microenvironment with the characteristics of the early stages of embryogenesis, EBs allow the lineage-specific differentiation. It has been already reported that the initial size of the 3D aggregates represents a critical factor that affects the germ layer selection controlling the late-stage differentiation: indeed, the EBs whose beginning dimensions are about 100 μm are more prone to express ectodermal markers, whereas the larger aggregates of 300–500 μm show an increased expression of mesodermal and endodermal markers (Park et al., 2007; Xu et al., 2011). Therefore, the formation of EBs with uniform sizes is important to drive a homogeneous and synchronous differentiation process. Our data, indeed, evidenced that the hFM-MSCs are inclined to form 3D aggregates of small dimensions that grew quite evenly, thus providing a microenvironment that facilitates the differentiation toward the neuronal lineage.

Unlike all the other reported protocols used to differentiate perinatal stem cells into neurons, which are based on the administration of RA and bFGF only, we mimicked *in vitro* all the steps involved in the *in vivo* MN development, adapting the protocol used for hESCs and hiPSCs (Maury et al., 2015) that encompasses an early neuralization, followed by caudalization and ventralization steps. Through this precise administration of small molecules and growth factors, that finely orchestrate the MN differentiation, hFM-MSCs underwent three different phases: their conversion into neuronal progenitors (4–5 days), the commitment into MN progenitors (4–5 days) and finally the maturation of post-mitotic MN (up to 40–50 days). During these three different steps, the expression of markers that have a critical role in the development of MNs (Thaler et al., 1999; deCastro et al., 2009; Alves et al., 2015; Varhaug et al., 2019) was monitored both at the transcriptional and protein levels. In particular, a basal expression of *PAX6* was detected in undifferentiated hFM-MSC, suggesting these cells are inclined to MN differentiation; moreover, the time course analysis of MN marker expression evidenced that *PAX6* and *ISL1* gradually increased during the first two weeks of culture and then decreased thereafter; differently, *HB9* that represents a late marker of MN differentiation, reached the highest expression at the end of differentiation process: these data are in accordance with Shimojo et al. that described a comparable trend of expression during the hiPSCs differentiation (Shimojo et al., 2015). After completing the differentiation process, the hFM-MSC derived MNs homogeneously showed the phenotype of mature MNs. Indeed, NF-L and tubulin β III, cytoskeletal components that provide structural support to neural cells, strongly marked the hFM-MSC derived MNs depicting their shape and size; HB9 and ISL-1, the homeobox genes crucial for the consolidation of spinal MN fate during development (Koronfel et al., 2021), continued to be expressed also in mature MNs displaying

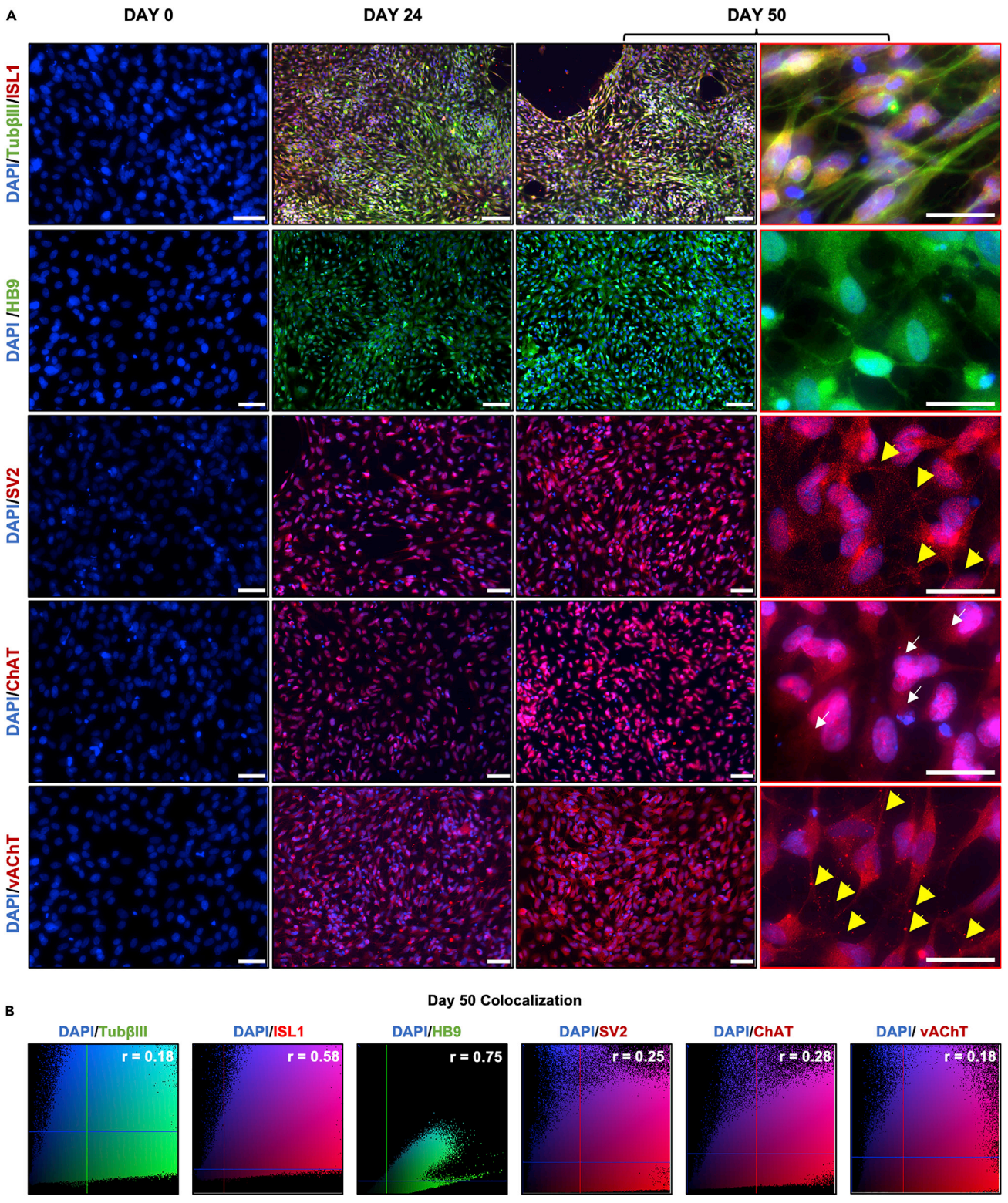

Figure 4. Time course of MN-specific markers expression

(A) Immunofluorescence for Tubulin βIII or HB9 in green fluorescence and of ISL1, SV2, ChAT and vAChT in red fluorescence in undifferentiated cells (day 0) and after 24 and 50 days of culture, as indicated. The nuclei were counterstained with DAPI (blue). Original magnification: 20x at day 0, 24 and 50, scale bar 100 μm; the last column shows details at bigger magnification (60x, scale bar 40 μm) of the day 50 staining. Images are representative of 5 independent

Figure 4. *Continued*
experiments White arrows indicate the peri-nuclear localization of ChAT, yellow arrowheads indicate the dotted pattern of vAChT or SV2 that mark the synaptic vesicles.
(B) ScatterPlot of the Day 50 colocalization between blue (nuclei) and green or red signal calculated using the Pearson's coefficient, as indicated.

predominantly nuclear localization (Leotta et al., 2014); ChAT, the enzyme responsible for the ACh biosynthesis, was mainly present in the perinuclear region of the ER and the Golgi complex: as these subcellular compartments are closely linked in their function in the newly synthesized proteins, the ChAT localization in the perinuclear compartment suggests an active synthesis of ACh in maturing hFM-MSC-derived MNs; finally, vAChT and SV2 localized, as expected, in the cytoplasm and along the axons, showing the typical vesicular staining pattern (Ichikawa et al., 1997). All these MNs markers were expressed in about 80% of the cells, evidencing that hFM-MSC can give rise to an MN progeny with an efficiency comparable to that of hiPSCs (Bianchi et al., 2018) and significantly higher than adult MSCs. Indeed, some laboratories reported a partial differentiation of bone marrow (BM)-MSCs into MN-like cells (Abdullah et al., 2016; Shirian et al., 2016; Sanooghi et al., 2021), demonstrated by expression of ChAT and ISL-1 in about 50% of the cell population, and whose functional activity was not characterized. The greater purity of hFM-MSCs derived progeny together with their higher proliferative rate (Ziadlou et al., 2015) and their increased immunomodulatory properties (Najar et al., 2010), suggest that placental stem cells might represent a tool more useful than BM-MSCs in the field of the neurosciences and of the neurodegenerative diseases.

MNs are excitable cells and to date one of the most challenging steps of MN differentiation is the obtaining of functional cells. Beyond morphological phenotyping, the electrophysiological characterization of stem cell derived MNs is indeed crucial to provide accurate measures of their function. MEA is particularly suited for these purposes because of its ability to record in real-time a large population of neurons and their network activity. In particular, MEA detects extracellular voltages, which reflect the spike activity of local neuronal populations. Here, we showed that the maturation phase of hFM-MSC-derived MNs is characterized by the acquisition of spontaneous electrical activity (as firing rate and bursts), as recorded by MEA. These findings are consistent with previous observations on hiPSC-derived MNs, in which the spike activity was recorded after 40–50 days of culture (Hu et al., 2010; Olmsted et al., 2022). The MN maturation over time was also reflected morphologically not only by the increased number, size, and complexity of neurites, that might suggest an enhanced ability of single MNs to develop action potentials, but also by the tendency of the neurons to group together forming cell clusters similar to that observed in hiPSC-derived MNs: this change in the spatial dimension, ensuring a closer proximity of the cells, might support their electrical maturation. Moreover, the increased expression over time of proteins related to the synthesis and transport of the ACh, such as ChAT or VAChT and SV2 suggests a progressive improvement of the neurotransmission capacity that would require 40–50 days to be efficient. The firing rate that we detected in hFM-MSC-derived MNs even if not particularly high, was still comparable to that observed in hiPSC-derived MNs (Smith et al., 2021; Thiry et al., 2022); but lower than that recorded in hiPSC-derived MNs co-cultured with astrocytes or *in vivo* (MNs isolated from animal spinal cord) (Carp et al., 2008; Taga et al., 2019): this finding probably reflects the absence in our system of neurotrophic influences from glial cells or of the neuromodulatory activity from afferent or descending inputs. In contrast with MEA studies utilizing cortical neurons (Odawara et al., 2018; Di Credico et al., 2021), we did not detect the formation of physiologically relevant neural networks among spinal cord hFM-MSC-derived MNs. Although a connection network among neurons was morphologically evident, the lack of a coordinated cluster of spiking across multiple electrodes is consisting in substantial regional differences between cortical and spinal cord neurons. Indeed, although the different cortical neuronal subtypes are prone to electrically connect each other giving rise to a complex network, the functional output of MNs is represented by the connection with myotubes rather than other neurons. Moreover, although the small molecule protocol for MNs differentiation may also generate ventral spinal interneurons able to synapse with MNs generating a network firing, the yield of such interneurons is very variable (Amoroso et al., 2013; Olmsted et al., 2022) and deeply conditioned by the concentration and the timing of treatments: it is then highly probable that DAPT concentration (10 uM) that we use to induce MNs differentiation may exert a cytotoxic effect not allowing a ventral spinal interneuron generation sufficient to coordinate a MNs spiking across electrodes (Butts et al., 2017). However, the lack of relevant neural networks is not an uncommon feature also in MEA studies performed on hiPSC-derived MNs, even in presence of astrocytes (Taga et al., 2019; Olmsted et al., 2022).

The functional goal of MNs is the formation of NMJ. Here we reported that hFM-MSC-derived MNs were able to interact with myotubes creating a functional NMJ, as demonstrated immunocytochemically and by

the contractile activity of myotubes. Indeed, we evidenced that the neuronal terminals ended on the myotube plasmalemma at the AChRs level. In mature NMJ, the AChRs are clustered underneath the motor nerve terminal, but in our co-culture, we detected only an attempt of AChR clusterization, showed by an increase of fluorescence in the point of contact with SV2, indeed the α-BTX predominately marked the C2C12 membranes. This is unsurprising because, in the immature myotubes, nicotinic AChRs are spread throughout the membrane, and only over time following signals from the motor nerve, they concentrate and anchor stably to the neuron contact site to potentiate the synaptic responsiveness (Zhang and Peng, 2011). However, even if the morphological maturation was not complete, the functional activity of the NMJ was proved by the increase in contractility of myotubes observed after about 1 week of co-culture (about 3 weeks after starting of the differentiation protocol), that was completely abolished by treatment with α-BTX, a well-known toxin that blocks the post-synaptic activity of AChRs (Hodgson, 2012). This observation is in line with previous data from hESCs- and hiPSCs-derived MNs, in which the functional NMJ is detected after about 1 week of co-culture with the myotubes (Puttonen et al., 2015; Yi et al., 2018). However, this timing seems in contrast with MEA analysis performed on the single cultures of hFM-MSC-derived MNs, in which the spontaneous electrical activity was recorded only after 40–50 days from the beginning of the differentiation protocol. Anyway, at the NMJ levels, there is bidirectional and physiologically relevant crosstalk between MNs and muscle cells, and skeletal muscle cells significantly contribute to neuronal physiology and electrical maturation (Madison et al., 2014; Rehorst et al., 2019). Finally, our experiments show that the obtained MNs can change the intracellular calcium homeostasis in C2C12 myotubes (Di Mauro et al., 2013); in particular, in the co-culture without a direct contact between MNs and myotubes the intracellular Ca^{2+} oscillations were very similar to each other, and both characterized by a slow oscillatory pattern. On the contrary, the direct contact between of hFM-MSC-derived MNs and C2C12 was able to induce intracellular Ca^{2+} variation characterized by a high frequency kinetic. The conversion in the intracellular calcium dynamics in the post-synaptic fiber is a key step and mutual contact is essential to NMJ-formation (Kaplan and Flucher, 2019).

In conclusion, our data strongly suggest that hFM-MSCs can generate a homogeneous population of functional MNs. These placental cells must be in the spotlight of cell therapy because of their various remarkable properties, such as self-renewal ability, lack of immunogenicity, strong secretory properties, and their plasticity to develop into different cell types. Unlike hiPSCs, the isolation and the maintenance of hFM-MSCs do not require specialized skills or excessive costs, suggesting these placental cells may represent a useful tool for *in vitro* disease modeling or drug screening. Moreover, even if additional *in vivo* analyses are required before encouraging their use for clinical purposes, these results indicate that hFM-MSCs might also represent a potential candidate for regenerative medicine in the field of neurodegenerative diseases, outlining an ethically acceptable strategy, that may overcome the risk of rejection or tumor formation.

Limitations of the study

- To evaluate the NMJ formation we established a xenoculture of hFM-MSCs derived MNs and murine myotubes: despite this represents a widely used culture method, it does not represent the physiological conditions: the replacement of the murine cells with human ones should be evaluated in future studies.
- *In vitro* differentiation of the hFM-MSC-derived MNs may not recapitulate all the features of the MNs development *in vivo*.
- Much efforts are needed to support the *in vitro* functional maturation of the hFM-MSC-derived MNs.
- Additional analyses about the cell survival/retention and engraftment after transplantation in animal models are required.

STAR★METHODS

Detailed methods are provided in the online version of this paper and include the following:

- KEY RESOURCES TABLE
- RESOURCE AVAILABILITY
  - Lead contact
  - Materials availability

SUPPLEMENTAL INFORMATION

Supplemental information can be found online at https://doi.org/10.1016/j.isci.2022.105197.

ACKNOWLEDGMENTS

This work was supported by PRIN Italian Ministry of University and Research (MUR), grant number PRIN20203AMKTW and ex 60% funds.

AUTHOR CONTRIBUTIONS

Conceptualization, A.D.B. and B.G.; investigation, G.G., A.D.C., S.G., and M.A.M.; formal analysis, G.G. and A.D.C.; data curation, G.G. and A.D.C.; writing – original draft G.G. and A.D.C.; writing – review and editing, P.B., A.D.B., and B.G.; supervision, A.D.B. and B.G.; project administration A.D.B. and B.G.

DECLARATION OF INTERESTS

The authors declare no competing interests.

Received: April 21, 2022
Revised: August 6, 2022
Accepted: September 21, 2022
Published: October 21, 2022

REFERENCES

Aasen, T., Raya, A., Barrero, M.J., Garreta, E., Consiglio, A., Gonzalez, F., Vassena, R., Bilić, J., Pekarik, V., Tiscornia, G., et al. (2008). Efficient and rapid generation of induced pluripotent stem cells from human keratinocytes. Nat. Biotechnol. *26*, 1276–1284. https://doi.org/10.1038/nbt.1503.

Abdullah, R.H., Yaseen, N.Y., Salih, S.M., Al-Juboory, A.A., Hassan, A., and Al-Shammari, A.M. (2016). Induction of mice adult bone marrow mesenchymal stem cells into functional motor neuron-like cells. J. Chem. Neuroanat. *77*, 129–142. https://doi.org/10.1016/j.jchemneu.2016.07.003.

Akazawa, C., Tsuzuki, H., Nakamura, Y., Sasaki, Y., Ohsaki, K., Nakamura, S., Arakawa, Y., and Kohsaka, S. (2004). The upregulated expression of sonic hedgehog in motor neurons after rat facial nerve axotomy. J. Neurosci. *24*, 7923–7930. https://doi.org/10.1523/JNEUROSCI.1784-04.2004.

Alves, C.J., Dariolli, R., Jorge, F.M., Monteiro, M.R., Maximino, J.R., Martins, R.S., Strauss, B.E., Krieger, J.E., Callegaro, D., and Chadi, G. (2015). Gene expression profiling for human iPS-derived motor neurons from sporadic ALS patients reveals a strong association between mitochondrial functions and neurodegeneration. Front. Cell. Neurosci. *9*, 289. https://doi.org/10.3389/fncel.2015.00289.

Amoroso, M.W., Croft, G.F., Williams, D.J., O'Keeffe, S., Carrasco, M.A., Davis, A.R., Roybon, L., Oakley, D.H., Maniatis, T., Henderson, C.E., and Wichterle, H. (2013). Accelerated high-yield generation of limb-innervating motor neurons from human stem cells. J. Neurosci. *33*, 574–586. https://doi.org/10.1523/JNEUROSCI.0906-12.2013.

Antonucci, I., Di Pietro, R., Alfonsi, M., Centurione, M.A., Centurione, L., Sancilio, S., Pelagatti, F., D'amico, M.A., Di Baldassarre, A., Piattelli, A., et al. (2014). Human second trimester amniotic fluid cells are able to create embryoid body-like structures in vitro and to show typical expression profiles of embryonic and primordial germ cells. Cell Transplant. *23*, 1501–1515. https://doi.org/10.3727/096368914X678553.

Bauer, U.S., Fiskum, V., Nair, R.R., van de Wijdeven, R., Kentros, C., Sandvig, I., and Sandvig, A. (2022). Validation of functional connectivity of engineered neuromuscular junction with recombinant monosynaptic pseudotyped ΔG-rabies virus tracing. Front. Integr. Neurosci. *16*, 855071. https://doi.org/10.3389/fnint.2022.855071.

Bianchi, F., Malboubi, M., Li, Y., George, J.H., Jerusalem, A., Szele, F., Thompson, M.S., and Ye, H. (2018). Rapid and efficient differentiation of functional motor neurons from human iPSC for neural injury modelling. Stem Cell Res. *32*, 126–134. https://doi.org/10.1016/j.scr.2018.09.006.

Butts, J.C., McCreedy, D.A., Martinez-Vargas, J.A., Mendoza-Camacho, F.N., Hookway, T.A., Gifford, C.A., Taneja, P., Noble-Haeusslein, L., and McDevitt, T.C. (2017). Differentiation of V2a interneurons from human pluripotent stem cells. Proc. Natl. Acad. Sci. USA *114*, 4969–4974. https://doi.org/10.1073/pnas.1608254114.

Carp, J.S., Tennissen, A.M., Mongeluzi, D.L., Dudek, C.J., Chen, X.Y., and Wolpaw, J.R. (2008). An in vitro protocol for recording from spinal motoneurons of adult rats. J. Neurophysiol. *100*, 474–481. https://doi.org/10.1152/jn.90422.2008.

de Castro, B.M., De Jaeger, X., Martins-Silva, C., Lima, R.D.F., Amaral, E., Menezes, C., Lima, P., Neves, C.M.L., Pires, R.G., Gould, T.W., et al. (2009). The vesicular acetylcholine transporter is required for neuromuscular development and function. Mol. Cell Biol. *29*, 5238–5250. https://doi.org/10.1128/MCB.00245-09.

Cave, C., and Sockanathan, S. (2018). Transcription factor mechanisms guiding motor neuron differentiation and diversification. Curr. Opin. Neurobiol. *53*, 1–7. https://doi.org/10.1016/j.conb.2018.04.012.

Chambers, S.M., Fasano, C.A., Papapetrou, E.P., Tomishima, M., Sadelain, M., and Studer, L. (2009). Highly efficient neural conversion of human ES and iPS cells by dual inhibition of SMAD signaling. Nat. Biotechnol. *27*, 275–280. https://doi.org/10.1038/nbt.1529.

Chatgilialoglu, A., Rossi, M., Alviano, F., Poggi, P., Zannini, C., Marchionni, C., Ricci, F., Tazzari, P.L., Taglioli, V., Calder, P.C., and Bonsi, L. (2017). Restored in vivo-like membrane lipidomics positively influence in vitro features of cultured mesenchymal stromal/stem cells derived from human placenta. Stem Cell Res. Ther. *8*, 31. https://doi.org/10.1186/s13287-017-0487-4.

Consentius, C., Reinke, P., and Volk, H.-D. (2015). Immunogenicity of allogeneic mesenchymal stromal cells: what has been seen *in vitro* and *in vivo*. Regen. Med. *10*, 305–315. https://doi.org/10.2217/rme.15.14.

Davis-Dusenbery, B.N., Williams, L.A., Klim, J.R., and Eggan, K. (2014). How to make spinal motor neurons. Development *141*, 491–501. https://doi.org/10.1242/dev.097410.

Di Baldassarre, A., Cimetta, E., Bollini, S., Gaggi, G., and Ghinassi, B. (2018). Human-induced pluripotent stem cell technology and cardiomyocyte generation: progress and clinical applications. Cells *7*, 48. https://doi.org/10.3390/cells7060048.

Di Credico, A., Gaggi, G., Izzicupo, P., Ferri, L., Bonanni, L., Iannetti, G., Di Baldassarre, A., and Ghinassi, B. (2021). Real-time monitoring of levetiracetam effect on the electrophysiology of an heterogenous human iPSC-derived neuronal cell culture using microelectrode array technology. Biosensors *11*, 450. https://doi.org/10.3390/bios11110450.

Di Mauro, M., Gallina, S., D'Amico, M.A., Izzicupo, P., Lanuti, P., Bascelli, A., Di Fonso, A., Bartoloni, G., Calafiore, A.M., and Di Baldassarre, A.; Italian Group of Study for Heart Valve Disease Italian Society of Cardiology (2013). Functional mitral regurgitation. Int. J. Cardiol. *163*, 242–248. https://doi.org/10.1016/j.ijcard.2011.11.023.

Díaz-Prado, S., Muiños-López, E., Hermida-Gómez, T., Rendal-Vázquez, M.E., Fuentes-Boquete, I., de Toro, F.J., and Blanco, F.J. (2011). Isolation and characterization of mesenchymal stem cells from human amniotic membrane. Tissue Eng. Part C Methods *17*, 49–59. https://doi.org/10.1089/ten.tec.2010.0136.

Du, Z.-W., Chen, H., Liu, H., Lu, J., Qian, K., Huang, C.-L., Zhong, X., Fan, F., and Zhang, S.-C. (2015). Generation and expansion of highly pure motor neuron progenitors from human pluripotent stem cells. Nat. Commun. *6*, 6626. https://doi.org/10.1038/ncomms7626.

Gaggi, G., Izzicupo, P., Di Credico, A., Sancilio, S., Di Baldassarre, A., and Ghinassi, B. (2019). Spare parts from discarded materials: fetal annexes in regenerative medicine. Int. J. Mol. Sci. *20*, 1573. https://doi.org/10.3390/ijms20071573.

Gaggi, G., Di Credico, A., Izzicupo, P., Antonucci, I., Crescioli, C., Di Giacomo, V., Di Ruscio, A., Amabile, G., Alviano, F., Di Baldassarre, A., and Ghinassi, B. (2020a). Epigenetic features of human perinatal stem cells redefine their stemness potential. Cells *9*, 1304. https://doi.org/10.3390/cells9051304.

Gaggi, G., Di Credico, A., Izzicupo, P., Alviano, F., Di Mauro, M., Di Baldassarre, A., and Ghinassi, B. (2020b). Human mesenchymal stromal cells unveil an unexpected differentiation potential toward the dopaminergic neuronal lineage. Int. J. Mol. Sci. *21*, 6589. https://doi.org/10.3390/ijms21186589.

Gaggi, G., Di Credico, A., Izzicupo, P., Sancilio, S., Di Mauro, M., Iannetti, G., Dolci, S., Amabile, G., Di Baldassarre, A., and Ghinassi, B. (2020c). Decellularized extracellular matrices and cardiac differentiation: study on human amniotic fluid-stem cells. Int. J. Mol. Sci. *21*, 6317. https://doi.org/10.3390/ijms21176317.

Gaggi, G., Di Credico, A., Guarnieri, S., Mariggiò, M.A., Di Baldassarre, A., and Ghinassi, B. (2022). Human mesenchymal amniotic fluid stem cells reveal an unexpected neuronal potential differentiating into functional spinal motor neurons. Front. Cell Dev. Biol. *10*, 936990. https://doi.org/10.3389/fcell.2022.936990.

Ghule, P.N., Medina, R., Lengner, C.J., Mandeville, M., Qiao, M., Dominski, Z., Lian, J.B., Stein, J.L., van Wijnen, A.J., and Stein, G.S. (2011). Reprogramming the pluripotent cell cycle: restoration of an abbreviated G1 phase in human induced pluripotent stem (iPS) cells. J. Cell. Physiol. *226*, 1149–1156. https://doi.org/10.1002/jcp.22440.

Harkness, L., Chen, X., Gillard, M., Gray, P.P., and Davies, A.M. (2019). Media composition modulates human embryonic stem cell morphology and may influence preferential lineage differentiation potential. PLoS One *14*, e0213678. https://doi.org/10.1371/journal.pone.0213678.

Hodgson, E. (2012). Toxins and venoms. In Progress in Molecular Biology and Translational Science (Elsevier), pp. 373–415.

Hu, B.-Y., Weick, J.P., Yu, J., Ma, L.-X., Zhang, X.-Q., Thomson, J.A., and Zhang, S.-C. (2010). Neural differentiation of human induced pluripotent stem cells follows developmental principles but with variable potency. Proc. Natl. Acad. Sci. USA *107*, 4335–4340. https://doi.org/10.1073/pnas.0910012107.

Ichikawa, T., Ajiki, K., Matsuura, J., and Misawa, H. (1997). Localization of two cholinergic markers, choline acetyltransferase and vesicular acetylcholine transporter in the central nervous system of the rat: in situ hybridization histochemistry and immunohistochemistry. J. Chem. Neuroanat. *13*, 23–39. https://doi.org/10.1016/S0891-0618(97)00021-5.

Itskovitz-Eldor, J., Schuldiner, M., Karsenti, D., Eden, A., Yanuka, O., Amit, M., Soreq, H., and Benvenisty, N. (2000). Differentiation of human embryonic stem cells into embryoid bodies compromising the three embryonic germ layers. Mol. Med. *6*, 88–95.

Kaplan, M.M., and Flucher, B.E. (2019). Postsynaptic CaV1.1-driven calcium signaling coordinates presynaptic differentiation at the developing neuromuscular junction. Sci. Rep. *9*, 18450. https://doi.org/10.1038/s41598-019-54900-w.

Koronfel, L.M., Kanning, K.C., Alcos, A., Henderson, C.E., and Brownstone, R.M. (2021). Elimination of glutamatergic transmission from Hb9 interneurons does not impact treadmill locomotion. Sci. Rep. *11*, 16008. https://doi.org/10.1038/s41598-021-95143-y.

Leotta, C.G., Federico, C., Brundo, M.V., Tosi, S., and Saccone, S. (2014). HLXB9 gene expression, and nuclear location during in vitro neuronal differentiation in the SK-N-BEneuroblastoma cell line. PLoS One *9*, e105481. https://doi.org/10.1371/journal.pone.0105481.

Madison, R.D., McGee, C., Rawson, R., and Robinson, G.A. (2014). Extracellular vesicles from a muscle cell line (C2C12) enhance cell survival and neurite outgrowth of a motor neuron cell line (NSC-34). J. Extracell. Vesicles *3*, 22865. https://doi.org/10.3402/jev.v3.22865.

Magatti, M., Stefani, F.R., Papait, A., Cargnoni, A., Masserdotti, A., Silini, A.R., and Parolini, O. (2019). Perinatal mesenchymal stromal cells and their possible contribution to fetal-maternal tolerance. Cells *8*, 1401. https://doi.org/10.3390/cells8111401.

Maraldi, T., Bertoni, L., Riccio, M., Zavatti, M., Carnevale, G., Resca, E., Guida, M., Beretti, F., La Sala, G.B., and De Pol, A. (2014). Human amniotic fluid stem cells: neural differentiation in vitro and in vivo. Cell Tissue Res. *357*, 1–13. https://doi.org/10.1007/s00441-014-1840-x.

Martelli, F., Ghinassi, B., Lorenzini, R., Vannucchi, A.M., Rana, R.A., Nishikawa, M., Partamian, S., Migliaccio, G., and Migliaccio, A.R. (2008). Thrombopoietin inhibits murine mast cell differentiation. Stem Cell. *26*, 912–919. https://doi.org/10.1634/stemcells.2007-0777.

Maury, Y., Côme, J., Piskorowski, R.A., Salah-Mohellibi, N., Chevaleyre, V., Peschanski, M., Martinat, C., and Nedelec, S. (2015). Combinatorial analysis of developmental cues efficiently converts human pluripotent stem cells

into multiple neuronal subtypes. Nat. Biotechnol. *33*, 89–96. https://doi.org/10.1038/nbt.3049.

Mitchell, K.E., Weiss, M.L., Mitchell, B.M., Martin, P., Davis, D., Morales, L., Helwig, B., Beerenstrauch, M., Abou-Easa, K., Hildreth, T., et al. (2003). Matrix cells from Wharton's jelly form neurons and glia. Stem Cell. *21*, 50–60. https://doi.org/10.1634/stemcells.21-1-50.

Moradi, S., Mahdizadeh, H., Šarić, T., Kim, J., Harati, J., Shahsavarani, H., Greber, B., and Moore, J.B. (2019). Research and therapy with induced pluripotent stem cells (iPSCs): social, legal, and ethical considerations. Stem Cell Res. Ther. *10*, 341. https://doi.org/10.1186/s13287-019-1455-y.

Najar, M., Raicevic, G., Boufker, H.I., Fayyad Kazan, H., De Bruyn, C., Meuleman, N., Bron, D., Toungouz, M., and Lagneaux, L. (2010). Mesenchymal stromal cells use PGE2 to modulate activation and proliferation of lymphocyte subsets: combined comparison of adipose tissue, Wharton's Jelly and bone marrow sources. Cell. Immunol. *264*, 171–179. https://doi.org/10.1016/j.cellimm.2010.06.006.

Nowack, A., Yao, J., Custer, K.L., and Bajjalieh, S.M. (2010). SV2 regulates neurotransmitter release via multiple mechanisms. Am. J. Physiol. Cell Physiol. *299*, C960–C967. https://doi.org/10.1152/ajpcell.00259.2010.

Odawara, A., Matsuda, N., Ishibashi, Y., Yokoi, R., and Suzuki, I. (2018). Toxicological evaluation of convulsant and anticonvulsant drugs in human induced pluripotent stem cell-derived cortical neuronal networks using an MEA system. Sci. Rep. *8*, 10416. https://doi.org/10.1038/s41598-018-28835-7.

Olmsted, Z.T., Stigliano, C., Marzullo, B., Cibelli, J., Horner, P.J., and Paluh, J.L. (2022). Fully characterized mature human iPS- and NMP-derived motor neurons thrive without neuroprotection in the spinal contusion cavity. Front. Cell. Neurosci. *15*, 725195. https://doi.org/10.3389/fncel.2021.725195.

Papait, A., Vertua, E., Magatti, M., Ceccariglia, S., De Munari, S., Silini, A.R., Sheleg, M., Ofir, R., and Parolini, O. (2020). Mesenchymal stromal cells from fetal and maternal placenta possess key similarities and differences: potential implications for their applications in regenerative medicine. Cells *9*, 127. https://doi.org/10.3390/cells9010127.

Park, J., Cho, C.H., Parashurama, N., Li, Y., Berthiaume, F., Toner, M., Tilles, A.W., and Yarmush, M.L. (2007). Microfabrication-based modulation of embryonic stem cell differentiation. Lab Chip *7*, 1018–1028. https://doi.org/10.1039/b704739h.

Pipino, C., Shangaris, P., Resca, E., Zia, S., Deprest, J., Sebire, N.J., David, A.L., Guillot, P.V., and De Coppi, P. (2013). Placenta as a reservoir of stem cells: an underutilized resource? Br. Med. Bull. *105*, 43–68. https://doi.org/10.1093/bmb/lds033.

Pittenger, M.F., Discher, D.E., Péault, B.M., Phinney, D.G., Hare, J.M., and Caplan, A.I. (2019). Mesenchymal stem cell perspective: cell biology to clinical progress. Npj Regen. Med. *4*, 22. https://doi.org/10.1038/s41536-019-0083-6.

Price, S.R., and Briscoe, J. (2004). The generation and diversification of spinal motor neurons: signals and responses. Mech. Dev. *121*, 1103–1115. https://doi.org/10.1016/j.mod.2004.04.019.

Puttonen, K.A., Ruponen, M., Naumenko, N., Hovatta, O.H., Tavi, P., and Koistinaho, J. (2015). Generation of functional neuromuscular junctions from human pluripotent stem cell lines. Front. Cell. Neurosci. *9*, 473. https://doi.org/10.3389/fncel.2015.00473.

Rehorst, W.A., Thelen, M.P., Nolte, H., Türk, C., Cirak, S., Peterson, J.M., Wong, G.W., Wirth, B., Krüger, M., Winter, D., and Kye, M.J. (2019). Muscle regulates mTOR dependent axonal local translation in motor neurons via CTRP3 secretion: implications for a neuromuscular disorder, spinal muscular atrophy. Acta Neuropathol. Commun. *7*, 154. https://doi.org/10.1186/s40478-019-0806-3.

Rennie, K., Gruslin, A., Hengstschläger, M., Pei, D., Cai, J., Nikaido, T., and Bani-Yaghoub, M. (2012). Applications of amniotic membrane and fluid in stem cell biology and regenerative medicine. Stem Cells Int. *2012*, 721538. https://doi.org/10.1155/2012/721538.

Rojas, P., Ramírez, A.I., Fernández-Albarral, J.A., López-Cuenca, I., Salobrar-García, E., Cadena, M., Elvira-Hurtado, L., Salazar, J.J., de Hoz, R., and Ramírez, J.M. (2020). Amyotrophic lateral sclerosis: a neurodegenerative motor neuron disease with ocular involvement. Front. Neurosci. *14*, 566858. https://doi.org/10.3389/fnins.2020.566858.

Rubino, E., Cruciani, M., Tchitchek, N., Le Tortorec, A., Rolland, A.D., Veli, Ö., Vallet, L., Gaggi, G., Michel, F., Dejucq-Rainsford, N., and Pellegrini, S. (2021). Human ubiquitin-specific peptidase 18 is regulated by microRNAs via the 3'Untranslated region, A sequence duplicated in long intergenic non-coding RNA genes residing in chr22q11.21. Front. Genet. *11*, 627007. https://doi.org/10.3389/fgene.2020.627007.

Saini, J., Faroni, A., Reid, A.J., Mouly, V., Butler-Browne, G., Lightfoot, A.P., McPhee, J.S., Degens, H., and Al-Shanti, N. (2021). Cross-talk between motor neurons and myotubes via endogenously secreted neural and muscular growth factors. Physiol. Rep. *9*, e14791. https://doi.org/10.14814/phy2.14791.

Bieback, K., and Brinkmann, I. (2010). Mesenchymal stromal cells from human perinatal tissues: from biology to cell therapy. World J. Stem Cells *2*, 81–92. https://doi.org/10.4252/wjsc.v2.i4.81.

Sanooghi, D., Vahdani, P., Bagher, Z., Faghihi, F., and Lotfi, A. (2021). In vitro characterization of human bone marrow mesenchymal stem cell-derived motor neurons induced by epigenetic modifiers. Egypt. J. Med. Hum. Genet. *22*, 53. https://doi.org/10.1186/s43042-021-00171-y.

Saykali, B., Mathiah, N., Nahaboo, W., Racu, M.-L., Hammou, L., Defrance, M., and Migeotte, I. (2019). Distinct mesoderm migration phenotypes in extra-embryonic and embryonic regions of the early mouse embryo. Elife *8*, e42434. https://doi.org/10.7554/eLife.42434.

Shimojo, D., Onodera, K., Doi-Torii, Y., Ishihara, Y., Hattori, C., Miwa, Y., Tanaka, S., Okada, R., Ohyama, M., Shoji, M., et al. (2015). Rapid, efficient, and simple motor neuron differentiation from human pluripotent stem cells. Mol. Brain *8*, 79. https://doi.org/10.1186/s13041-015-0172-4.

Shirian, S., Ebrahimi-Barough, S., Saberi, H., Norouzi-Javidan, A., Mousavi, S.M.M., Derakhshan, M.A., Arjmand, B., and Ai, J. (2016). Comparison of capability of human bone marrow mesenchymal stem cells and endometrial stem cells to differentiate into motor neurons on electrospun poly(ε-caprolactone) scaffold. Mol. Neurobiol. *53*, 5278–5287. https://doi.org/10.1007/s12035-015-9442-5.

Smith, A.S.T., Chun, C., Hesson, J., Mathieu, J., Valdmanis, P.N., Mack, D.L., Choi, B.-O., Kim, D.-H., and Bothwell, M. (2021). Human induced pluripotent stem cell-derived TDP-43 mutant neurons exhibit consistent functional phenotypes across multiple gene edited lines despite transcriptomic and splicing discrepancies. Front. Cell Dev. Biol. *9*, 728707. https://doi.org/10.3389/fcell.2021.728707.

Stifani, N. (2014). Motor neurons and the generation of spinal motor neuron diversity. Front. Cell. Neurosci. *8*, 293. https://doi.org/10.3389/fncel.2014.00293.

Taga, A., Dastgheyb, R., Habela, C., Joseph, J., Richard, J.-P., Gross, S.K., Lauria, G., Lee, G., Haughey, N., and Maragakis, N.J. (2019). Role of human-induced pluripotent stem cell-derived spinal cord astrocytes in the functional maturation of motor neurons in a multielectrode array system. Stem Cells Transl. Med. *8*, 1272–1285. https://doi.org/10.1002/sctm.19-0147.

Thaler, J., Harrison, K., Sharma, K., Lettieri, K., Kehrl, J., and Pfaff, S.L. (1999). Active suppression of interneuron programs within developing motor neurons revealed by analysis of homeodomain factor HB9. Neuron *23*, 675–687. https://doi.org/10.1016/S0896-6273(01)80027-1.

Thiry, L., Clément, J.P., Haag, R., Kennedy, T.E., and Stifani, S. (2022). Optimization of long-term human iPSC-derived spinal motor neuron culture using a dendritic polyglycerol amine-based substrate. ASN Neuro *14*. https://doi.org/10.1177/17590914211073381.

Varhaug, K.N., Torkildsen, Ø., Myhr, K.-M., and Vedeler, C.A. (2019). Neurofilament light chain as a biomarker in multiple sclerosis. Front. Neurol. *10*, 338. https://doi.org/10.3389/fneur.2019.00338.

Weiss, M.L., Medicetty, S., Bledsoe, A.R., Rachakatla, R.S., Choi, M., Merchav, S., Luo, Y., Rao, M.S., Velagaleti, G., and Troyer, D. (2006). Human umbilical cord matrix stem cells: preliminary characterization and effect of transplantation in a rodent model of Parkinson's disease. Stem Cell. *24*, 781–792. https://doi.org/10.1634/stemcells.2005-0330.

Witkowska-Zimny, M., and Wrobel, E. (2011). Perinatal sources of mesenchymal stem cells: Wharton's jelly, amnion and chorion. Cell. Mol. Biol. Lett. *16*, 493–514. https://doi.org/10.2478/s11658-011-0019-7.

Xu, F., Sridharan, B., Wang, S., Gurkan, U.A., Syverud, B., and Demirci, U. (2011). Embryonic stem cell bioprinting for uniform and controlled size embryoid body formation. Biomicrofluidics *5*, 022207. https://doi.org/10.1063/1.3580752.

Yang, H., Hao, D., Liu, C., Huang, D., Chen, B., Fan, H., Liu, C., Zhang, L., Zhang, Q., An, J., and Zhao, J. (2019). Generation of functional dopaminergic neurons from human spermatogonial stem cells to rescue parkinsonian phenotypes. Stem Cell Res. Ther. *10*, 195. https://doi.org/10.1186/s13287-019-1294-x.

Yi, H., Xie, B., Liu, B., Wang, X., Xu, L., Liu, J., Li, M., Zhong, X., and Peng, F. (2018). Derivation and identification of motor neurons from human urine-derived induced pluripotent stem cells. Stem Cells Int. *2018*, 3628578. https://doi.org/10.1155/2018/3628578.

Yu, C.-H., Davidson, S., Harapas, C.R., Hilton, J.B., Mlodzianoski, M.J., Laohamonthonkul, P., Louis, C., Low, R.R.J., Moecking, J., De Nardo, D., et al. (2020). TDP-43 triggers mitochondrial DNA release via mPTP to activate cGAS/STING in ALS. Cell *183*, 636–649.e18. https://doi.org/10.1016/j.cell.2020.09.020.

Zhang, H.L., and Peng, H.B. (2011). Mechanism of acetylcholine receptor cluster formation induced by DC electric field. PLoS One *6*, e26805. https://doi.org/10.1371/journal.pone.0026805.

Zhang, M., Wang, L., An, K., Cai, J., Li, G., Yang, C., Liu, H., Du, F., Han, X., Zhang, Z., et al. (2018). Lower genomic stability of induced pluripotent stem cells reflects increased non-homologous end joining. Cancer Commun. *38*, 49. https://doi.org/10.1186/s40880-018-0313-0.

Ziadlou, R., Shahhoseini, M., Safari, F., Sayahpour, F.-A., Nemati, S., and Eslaminejad, M.B. (2015). Comparative analysis of neural differentiation potential in human mesenchymal stem cells derived from chorion and adult bone marrow. Cell Tissue Res. *362*, 367–377. https://doi.org/10.1007/s00441-015-2210-z.

STAR★METHODS

KEY RESOURCES TABLE

REAGENT or RESOURCE	SOURCE	IDENTIFIER
Antibodies		
CD90-Alexa fluor 488-conjugated	Becton Dickinson	AB_395969
CD34-Alexa fluor 488-conjugated	Becton Dickinson	Cat#345801
CD45-Alexa fluor 488-conjugated	Becton Dickinson	Cat#345808
CD44-Alexa fluor 488-conjugated	Becton Dickinson	AB_395870
CD105-Alexa fluor 488-conjugated	Becton Dickinson	AB_10714629
CD14-Alexa fluor 488-conjugated	Becton Dickinson	Cat#347493
SSEA4-Alexa fluor conjugated	Becton Dickinson	Cat#560308
OCT4-Alexa fluor 488-conjugated	Becton Dickinson	Cat#5177
Tra-1–60-Alexa fluor 488-conjugated	Becton Dickinson	Cat#560173
C-KIT-PE-conjugated	Becton Dickinson	AB_400044
CD73-PE-conjugated	Becton Dickinson	Cat#561014
NANOG-Alexa fluor 647-conjugated	Becton Dickinson	Cat#560791
SOX2-Alexa fluor 488-conjugated	Becton Dickinson	Cat#561593
NF-L-Alexa Fluor 488 conjugated	Cell Signaling	Cat#8024
anti-HB9 Alexa Fluor 488 conjugated	Bioss Antibodies	Cat#Bs-11320R-A488
anti-VaChT	Sigma-Aldrich	Cat#SAB4200560
anti-Tubulin III	Sigma-Aldrich	Cat#T8578
anti-SV2	Invitrogen	Cat#PA5-52476
anti-ISL1 1	Invitrogen	Cat#PA5-27789
anti-ChAT	Abcam	Cat#ab22346
Chemicals, peptides, and recombinant proteins		
DMEM	Thermo Fisher Scientific	Cat#11965084
Neurobasal medium	Thermo Fisher Scientific	Cat#21103049
Advanced DMEM F12	Thermo Fisher Scientific	Cat#12634010
N2	Thermo Fisher Scientific	Cat#17502048
B27 without vitamin A	Thermo Fisher Scientific	Cat#A18956-01
B27	Thermo Fisher Scientific	Cat#17504-044
SB431542 hydrate	Sigma Aldrich	Cat#S4317-5MG
LDN193189	Stemgent	Cat#04-0074
CHIR-99021	Tocris	Cat#4423
retinoic acid	Sigma Aldrich	Cat#R2625
SAG	Sigma Aldrich	Cat#566660-1MG
Brain derived neurotrophic factor	R&D system	Cat#248-BD-005/CF
Glial cell line-derived neurotrophic factor	R&D system	Cat#212-GD-010
Ciliary neurotrophic factor	R&D system	Cat#130-096-336
IBMX	R&D system	Cat#2845
Forskolin	STEMCELL Technologies	Cat#72112
Critical commercial assays		
PowerUp SYBR Green Master mix	Thermo Fisher Scientific	Cat#A25742
High-Capacity cDNA reverse transcription kit	Thermo Fisher Scientific	Cat#4368814
FIX & PERM® Kit	Thermo Fisher Scientific	Cat#GAS004

(*Continued on next page*)

Continued

REAGENT or RESOURCE	SOURCE	IDENTIFIER
Experimental models: Cell lines		
hFM-MSCs	Isolated from placenta	NA
C2C12	ATCC	Cat# CRL-1772
Oligonucleotides		
See Table 2	NA	NA
Software and algorithms		
Prism	Prism-Graphad	https://www.graphpad.com/scientific-software/prism/

RESOURCE AVAILABILITY

Lead contact

Further information and requests for resources and reagents should be directed to and will be fulfilled by the lead contact: Angela Di Baldassarre.

Materials availability

This study did not generate unique reagents.

Data and code availability

- Data reported in this article will be shared by the lead contact on request.
- This article does not report original code.
- Any additional information required to reanalyze the data reported in this article is available from the lead contact on request.

EXPERIMENTAL MODEL AND SUBJECT DETAILS

Primary cell cultures

The study was approved by the local ethics committee. hFM-MSCs were isolated from 5 placentas obtained from 5 healthy donors by caesarean sections, after written informed consent in accordance with the Declaration of Helsinki, as previously described (Chatgilialoglu et al., 2017). Briefly, the amniochorionic membrane was separated from the chorion plate and washed in PBS phosphate-buffered saline (PBS, Corning, Somerville, MA, USA) supplemented with 1% of penicillin-streptomycin (Thermo Fisher Scientific, Waltham, MS, USA). The membrane was fragmented into small pieces and digested using a solution of 1 mg/mL collagenase type IV (Sigma-Aldrich, St. Louis, MO, USA) and 0.25% trypsin-EDTA (Corning) for 30 min at 37°C in agitation. After incubation, the digestion reaction was stopped by Fetal bovine serum (FBS, Corning) and the cells were centrifuged at 1200 rpm for 10 min. The pellet was resuspended and cultured in DMEM 10% FBS, supplemented with 1% penicillin/streptomycin and 2 mM L-glutamine (all purchased from Thermo Fischer Scientific).

Cell lines

C2C12 cell line was purchased from ATCC (Mannassan, VA, USA) and cultured in DMEM 10% FBS, supplemented with 1% penicillin/streptomycin and 2 mM L-glutamine. For myotube differentiation, when C2C12 reached the 90% of confluence, the medium was switched into DMEM 2% FBS for 5–6 days. All the cell cultures were maintained at 37°C and 5% CO_2.

METHOD DETAILS

Flow cytometry

Phenotypical characterization of hFM-MSCs was performed between passages 2 and 4. Briefly, cells were treated with the FIX & PERM® Kit (Thermo Fisher Scientific) and then incubated for 1 h at RT with human anti-CD90-Alexa Fluor 488-conjugated, CD34-Alexa Fluor 488-conjugated, CD45-Alexa Fluor 488-conjugated, CD44-Alexa Fluor 488-conjugated, CD105-Alexa Fluor 488-conjugated, CD14-Alexa Fluor

488-conjugated, SSEA4-Alexa Fluor conjugated, OCT4-Alexa Fluor 488-conjugated, Tra-1–60-Alexa Fluor 488-conjugated, C-KIT-PE-conjugated, CD73-PE-conjugated, NANOG-Alexa Fluor 647-conjugated, SOX2-Alexa Fluor 488-conjugated (All from Becton Dickinson, Franklin Lakes, NJ, USA) diluted 1:50–1:100 according to the manufacturer's instructions. Cells incubated with isotypes (all from Becton Dickinson) were used as negative controls.

Cytometric analysis was performed with a CytoFLEX Cytometer (Beckman Coulter Pasadena, CA, USA), and data were analyzed with CytExpert Acquisition and Analysis Software (Beckman Coulter).

Motor neuron differentiation

EBs were generated seeding the hFM-MSCs at high density (6×10^5 cell/mL) in ultra-low attachment 6 well plates (Corning, Flintshire, USA) in N2B27 medium [DMEM F12:Neurobasal vol:vol supplemented with N2, B27 minus vitamin A and β-mercaptoethanol (βMOH 0.1mM) (all purchased sed from Thermo Fisher Scientific, Waltham, MA, USA)] and sequentially exposed to SB431542 hydrate (10 μM, Sigma-Aldrich, Saint Louis, MO, USA), LDN193189 (100 nM, Stemgent, Cambridge, MA, USA), CHIR-99021 (3 μM, Tocris Bioscience, Bristol, UK), bFGF (10 ng/mL, Thermo Fisher Scientific), ascorbic acid (AA, 10 μM, Sigma-Aldrich), retinoic acid (RA, 100nM, Sigma-Aldrich), SAG (500 nM, Sigma-Aldrich), DAPT (10 μM, Tocris Bioscience), Brain derived neurotrophic factor (BDNF, 10 ng/mL, R&D system, Minneapolis, MN, USA), Glial cell line-derived neurotrophic factor (GDNF, 20 ng/mL, R&D system) and ciliary neurotrophic factor (CTNF, 10 ng/mL R&D system).

At day 16, EBs were dissociated with 0.05% trypsin (Thermo Fisher Scientific) and DNAse I solution 50 mg/mL (STEMCELL Technologies, Vancuver, Canada) and the seeded at $1.5 \times 10^5/cm^2$ in plates precoated with polyornithine (20 μg/mL)/laminin (3 μg/mL) in NDM medium [Neurobasal medium, 1% penicillin/streptomycin, 2 mM L-glutamine, N2, non-essential aminoacids 1x] supplemented with BDNF 10 ng/mL, GDNF 20 ng/mL, CTNF 10 ng/mL (R&D system), βMOH (25 μM, Sigma-Aldrich), Forskolin (10 μM, STEMCELL Technologies), IBMX (100 μM, R&D system), Glutamate (GluE, 25μM, Sigma-Aldrich) and Uridine/Fluorodeoxyuridine (UFUDU, 1 μM, Sigma-Aldrich) (Figure S1).

Co-culture of hFM-MSC-derived MNs and myotubes

After EBs dissociation, hFM-MSC-derived MNs (day 16) were seeded on differentiated myotubes in NDM medium supplemented as reported above. For the non-contacting co-culture, cells were cultured in a μ-slide co-culture dish (ibidi GmbH, Gräfelfing, Germany). When required, hFM-MSC-derived MNs were loaded with the long-lasting vital dye ViaFluor SE 405 5 μM (Biotium Inc, Fremont, CA, USA) before the plating on the myotubes.

RNA extraction and reverse transcription

Cells were lysed with QIAzol lysis reagent (QIAGEN, Germany) and the total RNA was extracted using the miRNeasy Mini Kit (QIAGEN) according to the manufacturer's procedure. For reverse transcription, 1 μg of RNA was retrotranscribed by the High-Capacity cDNA reverse transcription kit (Thermo Fisher Scientific) (Martelli et al., 2008).

Real time quantitative PCR (qPCR)

qPCR analysis was performed using SYBR green (PowerUp SYBR Green Master mix, Thermo Fisher Scientific) as previously described (Gaggi et al., 2020b). The run method consisted of the following steps: 95°C for 10 min, 95°C for 15 s, 60°C for 1 min. Steps 2 and 3 were repeated for 40 cycles. The authenticity of the PCR products was verified by melt-curve analysis. Each gene expression value was normalized to 18S. Because some MN-specific genes were undetectable at day 0, the fold changes were expressed in relation to day 14, as previously reported by Shimojo et al. (2015) using the ΔΔCt method. The primers used are listed in Table 3.

Morphological analysis

Immunofluorescence analysis was performed as previously described (Gaggi et al., 2020c). Briefly, cells were fixed with 4% paraformaldehyde for 10 min, permeabilized with 0.5% Triton X-100 for 15 min and incubated in 5% bovine serum albumin (BSA) for 20 min at room temperature to avoid unspecific bindings. Cells were subsequently incubated with anti-NF-L-Alexa Fluor 488 conjugated (1:50, Cell Signaling Danvers, MA,

USA), anti-HB9 Alexa Fluor 488 conjugated (1:50, Cell Signaling Danvers), anti-VaChT (1:100, Sigma-Aldrich), anti-Tubulin βIII (1:50, Sigma-Aldrich), anti-SV2 (1:100, Invitrogen, Carlsbad, CA, USA), anti-ISL1 1 (1:100, Invitrogen), anti-ChAT (1:100, Abcam) followed by the appropriate secondary antibody conjugated with Alexa Fluor 546 or Alexa Fluor 488 (1:100, Invitrogen, Carlsbad, CA, USA). Nuclei were counterstained with DAPI (Thermo Fisher Scientific).

To detect the presence of the neuromuscular junction, MN-like cells were stained with ViaFluor SE 405 5 μM (Biotium Inc) following the manufacturer's procedure, or anti-SV2 followed by the secondary antibody Alexa Fluor 546 conjugated, whereas the myotubes were stained with α-BTX Alexa Fluor 488 conjugated (Thermo Fisher Scientific). Images were acquired confocal microscope Zeiss LSM800 microscope equipped with an inverted microscope Axio-observer D1 and an objective W-Plan-Apo X/1.3 DIC (Carl Zeiss, Jena, Germany) and analyzed with ZEN Software (Carl Zeiss).

The image analyses were performed by Celleste Image Analysis Software (Thermo Fisher Scientific).

Contraction analysis

The degree of muscle contraction was quantified by the tracking distance tool of the Celleste Image Analysis Software (Thermo Fisher Scientific): This option allows to automatically select all moving objects contained in the region of interest and tracking their movements over time. The distance covered by each point of the contracting myotubes provides an indirect quantification of the contraction. Numerical data were exported from the datatable option and used for statistical analysis. In addition, graphs were obtained to visually represent the myotubes contraction. The distance was expressed as pixel (y-axis) over time (x-axis). The selected regions of interest were maintained constant to permit the comparison among the different experimental conditions. The videos were uploaded in the analysis software as MP4 extension.

Alpha-bungarotoxin assay

The α-BTX assay was performed as previously reported (Saini et al., 2021; Bauer et al., 2022). Briefly, a video of contraction activity was recorded for 18s, then it was stopped and α-BTX 1:300 (Thermo Fisher Scientific) was added to the cell culture and incubated for 10 min at 37°C. Subsequently the contraction activity was monitored for further 2 minutes and recorded for 10s.

Calcium imaging

Intracellular Ca^{2+} levels were monitored in single culture of myotubes and in contacting and non-contacting coculture of myotubes and differentiating hFM-MSCs by using the dye Fluo4-acetoxymethyl ester (Fluo4/AM, Thermo Fisher Scientific). An upright microscope (Zeiss Axio Examiner; Carl Zeiss) was used, equipped with 40 ×0.75 NA water-immersion objectives connected by optical fiber to a 75 W Xenon lamp and a monochromator (OptoScan; Cairn Instrument, UK). Sub-millisecond bandpass and wavelength controls were used with a back-illuminated camera (EMCCD, Evolve 512; Photometrics, Tucson, USA). The cells were incubated with 5 μM Fluo-4/AM in normal external solution (NES: 140 mM NaCl, 2.8 mM KCl, 2 mM $CaCl_2$, 2 mM $MgCl_2$, 10 mM glucose, 10 mM Hepes, pH 7.3) supplemented with 1% (w/v) bovine serum albumin for 40 min at 37°C. Recordings on Fluo4-loaded cells were performed in NES. The fluorescence was acquired by setting excitation at 488 nm and images acquired at 20 frames/s with an EMCCD camera and stored on an interfaced computer for off-line analysis using MetaFluor (Molecular Device, Sunnyvale, CA, USA). The temporal analysis was calculated as the mean fluorescence intensity signal in a selected cell area, as F/F_0, where F is the fluorescence emission of a single loaded cell acquired during a time lapse, and F_0 is the mean fluorescence intensity of the same cell calculated from first images acquired.

Multi-electrode array (MEA) recordings and data processing

At day 16, hFM-MSC-derived MN-like cells were dissociated and seeded (10×10^5 cell/well) on a precoated (polyornithine/laminin) 24-Well CytoView MEA plate (M384-tMEA-24W, Axion Biosystems) to record spontaneous electrical activity. Experiments were performed using Maestro Edge (Axion Biosystems) MEA System as previously described (Di Credico et al., 2021). During the recordings, cells were maintained at 37°C/5% CO_2. All data were acquired by Axion Integrated Studio (Axis) Navigator 3.2.3.1 software (Axion Biosystems). Sampling frequency was set at 12.5 kHz. Briefly, Neural Real-Time module with spontaneous configuration was selected to record the spontaneous neuronal activity. Adaptive Threshold Crossing

method, in which the threshold to detect a spike was set 6x Std Dev of the noise, was selected to detect spiking activity. Inter-Spike Interval (ISI) Threshold was used to detect single-electrode bursting activity, setting the minimum number of spikes at 5 and the maximum ISI at 100 ms, as suggested by manufacturer. After the recordings, data analyzed by the Neural Metric Tool (Axion Biosystems) and the Envelope algorithm was selected analyze the network bursting activity. The analyzed variables were the mean firing rate averaged across the active electrodes (i.e., weighted mean firing rate - MFR), the burst frequency (i.e., total number of bursts divided by the duration of the analysis), and the burst duration (i.e., average time from the first spike to last spike in a burst). Statistical analysis was performed using PRISM 9.2.

QUANTIFICATION AND STATISTICAL ANALYSIS

All data are presented as the mean $\pm$ SD. A statistical analysis was performed using the one-way analysis of variance (ANOVA) and Tukey's post-hoc analysis. The level of significance was set at $p < 0.05$.